DEPARTMENT OF MATHEMATICS

Backwater Analysis for Channel Flows and Side-weirs using IDES.

by

A. Priestley

Numerical Analysis Report **7/92**

UNIVERSITY OF READING

Final Report on the Contract entitled "Backwater Analysis for Channel Flows and Side-weirs using IDES" for HR Wallingford Ltd..*

A. Priestley

Institute for Computational Fluid Dynamics,

Department of Mathematics,

University of Reading,

Whiteknights,

Reading,

United Kingdom.

September 30, 1992

*The work reported here forms part of the research programme of the Reading/Oxford Institute for Computational Fluid Dynamics and was funded by HR Wallingford Ltd..

Contents

List of Figures

List of Tables

0 Abstract

In this report we will investigate the use of Implicit Differential Equation Solvers (IDES) for solving steady-state problems of the type considered in the HR Wallingford CHAT software package. In particular we will perform backwater analyses for channels and for channels with sideweirs. That is, given conditions at outlet we calculate the flow in the rest of the channel and, in particular, at inlet. The method solves both sub and super-critical flows and a possible treatment for the trans-critical case will also be presented.

1 Introduction

It has been traditional to write Ordinary Differential Equations (ODEs) in the form

$$y\prime = f(x, y) \tag{1.1}$$

where x is the independent variable and y is the solution. Solution techniques for this type of equation are well-known and well documented, see Henrici [4] or Lambert [5] for example. Rather less well-known, Fox & Mayers [3], are solution techniques that deal with equations of the form

$$F(x, y, y\prime) = 0 \tag{1.2}$$

$$\text{or} \qquad y\prime = f(x, y, y\prime). \tag{1.3}$$

We will refer to these solution techniques as Implicit Differential Equation Solvers, or IDES for short. Equations in the form (1.1) have obvious advantages, but there may be situations where it is preferable to use the form represented in (1.3). The obvious case is when the function, F in (1.2), is just not separable due to nonlinearity in the term $y\prime$.

In the case of shallow water flow the equation governing steady-state flow can, typically, be written as

$$y\prime = \frac{S_0 - S_f}{1 - F_r^2} \tag{1.4}$$

where y is now the depth of water in the channel or pipe etc., S_0 is the bed-slope, S_f is a friction term and F_r is the Froude number which is a function of depth, massflow and the channel geometry. Problems arise, though, in computations when F_r passes through unity, that is the flow changes from sub-critical flow to super-critical flow, or indeed if F_r just gets sufficiently close to 1, as in these cases the right hand side of (1.4) becomes unbounded for computational purposes. The division by the factor $1 - F_r^2$ is rather artificial and the equation more naturally appears as

$$y\prime = F_r^2 y\prime + S_0 - S_f. \tag{1.5}$$

The division by $1 - F_r^2$ is just performed to get the equation into the form of (1.1).

The equation was first solved in the form (1.5) by Chawdhary [1] and also appeared in Samuels & Chawdhary [7]. We shall give details of the algorithm in the next sections and will show that the method is capable of giving accurate results for backwater analyses of both sub-critical and super-critical flows. The results in [1] and [7] indicate that the method also deals with the trans-critical case. Certainly this work shows that the method does not fail as the critical point is reached but we argue that in the cases considered here another boundary condition is required to give the problem a unique solution. (It is possible that the trans-critical case was successfully solved in [1] because the jumps were forced by changes in the bed-slope). The important point, though, is that IDES are capable of solving sub- and super-critical backwater problems and will not blow up as a critical point is approached.

In the next section we describe, in detail, how to apply the problem to a rectangular cross-section channel problem and we then follow this by solving the rather more difficult side-weir problem. Numerical results will be given in both sections. The work will then be summarised.

2 Channel Flow

The equations governing steady-state flow in a rectangular cross-section channel are that the massflow, $Q = uA$, is a constant with u being the velocity and $A = By$ the cross-sectional wetted area with B the channel breadth, and that the depth y satisfies the differential equation

$$y\prime = \frac{\alpha Q^2}{gB^3y^2}\frac{dB}{dx} + \alpha F_r^2 y\prime + S_0 - S_f. \tag{2.6}$$

The parameter α models energy loss that is sometimes included in the shallow water equations. It will here be assumed to be a constant, usually 1, although, again, this is no limitation on the method. The friction slope, S_f, can be prescribed as desired, but here we shall typically be using Manning's equation,

$$S_f = \frac{Q|Q|n^2(2y+B)^{4/3}}{(By)^{10/3}},$$

where n is some constant. The acceleration due to gravity is denoted by g.

The notation, and convention, that we will use throughout this report is that x increases from left to right and we discretize the equation (2.6)

at certain, not necessarily equi-spaced, points x_n. The distance between x_n and x_{n+1} is denoted by $\Delta x_{n+\frac{1}{2}}$. Without loss of generalization this will be assumed to take a constant value Δx. The solution at these points is then denoted by y^n. As we are solely concerned with backwater analyses in this report we will therefore assume that y^{n+1} is known and y^n is to be found. To find y^n we perform an iteration on this value and we will denote the k^{th} approximation to y^n simply by y^k, the value of n being understood. As we are assuming that the channel only has linearly varying breadth the term dB/dx will be replaced by the constant β. The bed-slope, S_0, will also be a constant for our calculations here, but this is not a restriction of the method, [1]. Following Chawdhary [1] equation (2.6) is now discretised, using the trapezium rule, in the form

$$\frac{y^{n+1}-y^{k+1}}{\Delta x} = \frac{\beta Q^2}{2g}\left\{\frac{1}{B_{n+1}^3 y^{n+1^2}} + \frac{1}{B_n^3 y^{k^2}}\right\} + \frac{\alpha}{2}\left(F_r^{k^2} + F_r^{n+1^2}\right)\frac{y^{n+1}-y^k}{\Delta x} + S_0 - \frac{1}{2}(S_f^k + S_f^{n+1}).$$

With a little re-arrangement the scheme then becomes,

$$y^0 = y^{n+1}$$

$$y^{k+1} = y^{n+1} - \frac{\Delta x \beta Q^2}{2g}\left\{\frac{1}{B_{n+1}^3 y^{n+1^2}} + \frac{1}{B_n^3 y^{k^2}}\right\} - \frac{\alpha}{2}\left(F_r^{k^2} + F_r^{n+1^2}\right)\left(y^{n+1} - y^k\right) - \Delta x S_0 + \frac{\Delta x}{2}\left((S_f^k + S_f^{n+1}\right) \quad \text{for} \quad k = 0, 1, 2, \ldots \tag{2.7}$$

The condition that ensures the iteration (2.7) converges is simply that

$$\left|\frac{\partial y^{k+1}}{\partial y^k}\right| < 1. \tag{2.8}$$

In principle we could calculate (2.8) exactly for the iteration (2.7), but the expression would be cumbersome. However, the terms we might wish to avoid are all multiplied by Δx. Hence they can be made as small as we wish ($y \neq 0$) by control of the space step Δx. We shall argue later that it is beneficial for other reasons to use what computational time is available solving on a finer mesh, rather than using the same time on a more complex iterative scheme with a coarser mesh. The term we cannot control in this fashion is the one involving the Froude number. Hence for super-critical flow, or more generally when $\alpha F_r^2 > 1$, we re-arrange (2.6) as

$$y' = \frac{1}{\alpha F_r^2}\left(y' - \frac{\beta\alpha Q^2}{gB^3y^2} - S_0 + S_f\right).$$

This can then be discretised in the same manner as (2.7). The Froude number is a quantity that will need to be calculated anyway and so this approach results in little extra computational cost.

Not too many results will be given in this section as very complete numerical results will be included in the next section, for the harder side-weir problem, with errors and convergence histories. Here, though, we just give some results to demonstrate the main types of flow that occur. For all the results Manning's constant, n, takes a value of 0.01 and the energy loss factor, α, takes a value of 1.

The first situation is shown in figure 1 and shows a sub-critical flow. Figure 2 shows a super-critical flow in a similar channel. Figure 3 gives the

results for a trans-critical situation.

In figures 4 and 5 we see a sub-critical and super-critical flow in a channel with an adverse slope.

The convexity of these solutions agrees with those given in Chow [2]. The accuracy of the method will be discussed more fully in the context of the solutions to the side-weir problem.

There are two situations where the code fails. Both cases are when there is no physical flow along the entire channel with the given outflow conditions. As the flows are unphysical it would be pointless, and wrong, to attempt any mathematical/numerical treatment. However, as far as CHAT is concerned something must be done to ensure that the code is robust. Firstly, and rather obviously, these occasions must be accompanied by severe error messages as not only is the flow in this particular channel unphysical but any calculation upstream of this channel is also rather meaningless. The first unphysical case is that of a flow that is super-critical at outflow but is not sufficiently 'strong' to reach inflow super-critically. As the calculation proceeds the flow becomes critical in the interior of the channel. The obvious 'fix' is to continue the solution from this point to inflow at the critical depth. The problem with this is that if this critical depth is also the critical depth for the next channel then problems are likely to arise with unphysical flows in this channel as well. Given that the flow is unphysical, considered as a whole anyway this is perhaps not too serious. The alternative

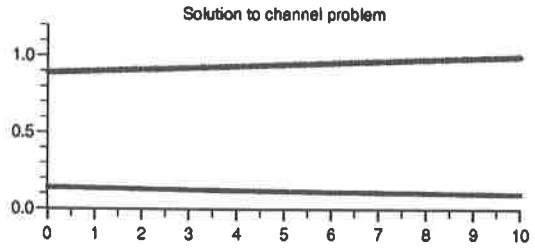

Figure 1: Depth and Froude no. for sub-critical flow in a channel. Slope = 0.01, width = 1m, 200 points. Outflow depth is 1m with inflow depth 0.8918m. Massflow = $1m^3s^{-1}$.

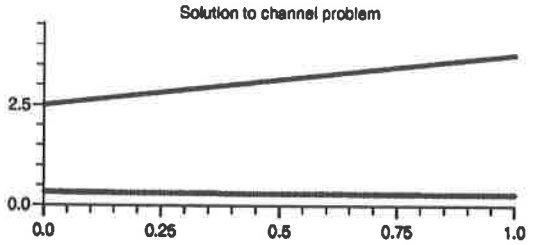

Figure 2: Depth and Froude no. for super-critical flow in a channel. Slope = 0.1, width = 1m, 200 points. Outflow depth is 0.3m with inflow depth 0.34368m. Massflow = $1m^3s^{-1}$.

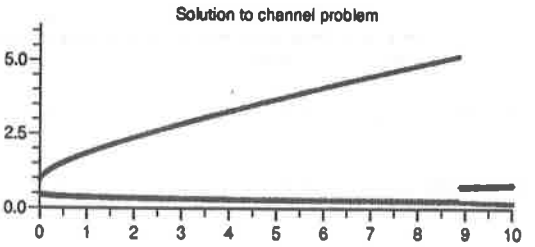

Figure 3: Depth and Froude no. for trans-critical flow in a channel. Slope = 0.04, width = 1m, 200 points. Outflow depth is 0.8m with inflow depth 0.463784m. Massflow = $1m^3s^{-1}$.

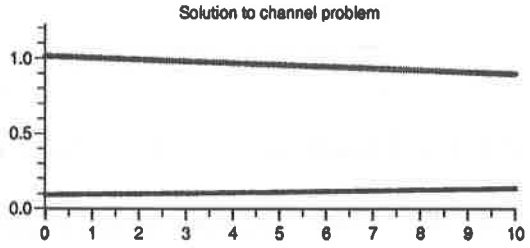

Figure 4: Depth and Froude no. for sub-critical flow in a channel. Slope = -0.01, width = 1m, 200 points. Outflow depth is 0.9m with inflow depth 1.0186m. Massflow = $1m^3s^{-1}$.

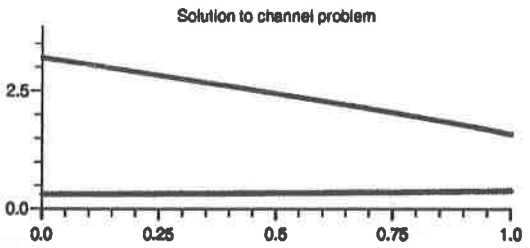

Figure 5: Depth and Froude no. for super-critical flow in a channel. Slope = -0.1, width = 1m, 200 points. Outflow depth is 0.4m with inflow depth 0.3165m. Massflow = $1m^3s^{-1}$.

is to put the remaining values equal to the normal depth. (Note: It may be that where friction is included this case becomes physical. The numerical scheme is actually quite capable of calculating through the critical value and hence the calculation of this case presents no problems.) The second case is when there is sub-critical flow at outflow but this again reaches critical depth somewhere in the interior and there is no physical jump, at any point of the sub-critical flow, that produces a super-critical flow strong enough to reach inflow. In this case it would seem most natural to include an unphysical jump down to the normal depth and continue the solution to inflow with this value.

These comments are equally valid for channels with side-weirs.

3 Side-weirs

For a derivation of the equations governing the flow in a channel with a side-weir the reader is again refered to Chow [2]. These equations, in which massflow is no longer a constant and also has to be solved for, are, where we no longer assume a channel of uniform width as in [2],

$$\frac{dy}{dx} = \frac{S_0 - S_f - \alpha Q Q_x / g A^2 + \alpha F^2 y B\prime / B}{(1 - \alpha F_r^2)}, \tag{3.9}$$

and, for the massflow,

$$(Q_{weir})_x = -Q_x = c\sqrt{2g}(y - s)^{3/2}. \tag{3.10}$$

In equation (3.10) c is the weir coefficient, taken to have a value of 0.9 in all our calculations, and s is the height of the weir sill above the bed-level. In this report we will take $s = \frac{1}{2}m$. Equations (3.9) and (3.10) represent the most complex situation, to be encountered in CHAT. Before proceeding to solve these equations we can attempt a simpler problem that has an analytical solution. This is achieved by setting

$$S_0 = 0$$

$$S_f = 0$$

$$\text{and} \quad \alpha = 1.$$

Assuming energy, e, to be constant in the channel, Chow [2], we can write

$$e = y + \frac{u^2}{2g}$$

$$= y + \frac{Q^2}{2A^2g}$$

$$\Longrightarrow Q = \sqrt{A^2 2g(e-y)}. \tag{3.11}$$

Substituting for Q and Q_x from (3.11) and (3.10) into equation (3.9) we get,

$$\frac{dy}{dx} = \frac{2c}{B}\frac{\sqrt{(e-y)(y-s)^3}}{(3y-2e)}. \tag{3.12}$$

Equation (3.12) is now a single ODE for a single unknown, y, and furthermore it is separable. Writing

$$\begin{aligned} y &= e\cos^2(\theta) + s\sin^2(\theta) \\ e - y &= (e-s)\sin^2(\theta) \\ y - s &= (e-s)\cos^2(\theta) \\ dy &= -2(e-s)\sin(\theta)\cos(\theta)d\theta \end{aligned}$$

and we can then show that

$$\begin{aligned} \int \frac{(3y-2e)}{(e-y)^{1/2}(y-s)^{3/2}}dy &= \int \frac{(3e\cos^2(\theta) + 3s\sin^2(\theta) - 2e)[-2(e-s)]\sin(\theta)\cos(\theta)}{(e-s)^2\sin(\theta)\cos^3(\theta)}d\theta \\ &= \frac{-2}{e-s}\int \left(3e\cos^2(\theta) + 3s\sin^2(\theta) - 2e\right)\frac{d\theta}{\cos^2(\theta)} \\ &= \frac{-2}{e-s}\int \left(3e + 3s\tan^2(\theta) - 2e\sec^2(\theta)\right)d\theta \\ &= \frac{-2}{e-s}\left[3e\theta + 3s(\tan(\theta) - \theta) - 2e\tan(\theta)\right] \end{aligned}$$

and hence

$$\frac{2cx}{B} + constant = \frac{-2}{e-s}\left[3(e-s)\theta + (3s-2e)\tan(\theta)\right] \qquad (3.13)$$

where

$$\cos(\theta) = \sqrt{\frac{y-s}{e-s}}.$$

Although (3.13) is not quite in the form we would wish, with x being given as a function of y rather than the other way round, this formula is quite simple to invert given the monotonicity of the solution, Porter [6], and can be solved to any required degree of accuracy. The constant is determined by the length of channel and the depth and massflow (hence the energy e) at outflow.

We will now look at the accuracy of the method for the three types of flow that can occur, sub-critical, super-critical and trans-critical. The three test problems all consist of a 5m channel that is 1m wide. Sill height and other parameters are selected as described before. Outflow depth is taken to be 0.7m, that is 20cm above the sill height. The three problems can now be distinguished by just specifying the massflow at outflow. For the first (sub-critical) problem we take $Q = 0.01m^3s^{-1}$, for the second, super-critical, case we take $Q = 6.0m^3s^{-1}$ and finally for the trans-critical case $Q = 1.0m^3s^{-1}$. The exact solution, as calculated from equation (3.13), to problem 1 is shown in figure 6, the exact solution to problem 2 in figure 7 and the exact solution to problem 3 in figure 8.

Problem 3 does not actually have an unique exact solution. Another condition, usually from inflow, is needed to make the solution unique. The condition we have chosen here is that the jump should be the smallest possible to produce a flow that reaches inflow physically. Although this does not preclude shocks that jump to a value above the sill height, with the channel set up as it is these situations invariably become unphysical before inflow is reached. Once a shock that jumps to the sill height is produced the upstream solution is then

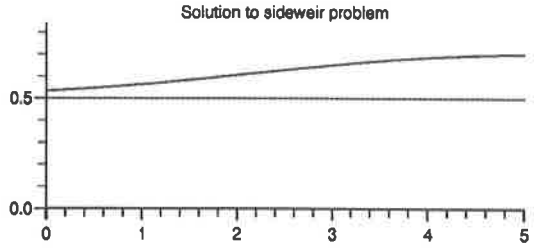

Figure 6: Depth for Problem 1. Inflow depth and massflow are 0.534426m and $0.962776 m^3 s^{-1}$.

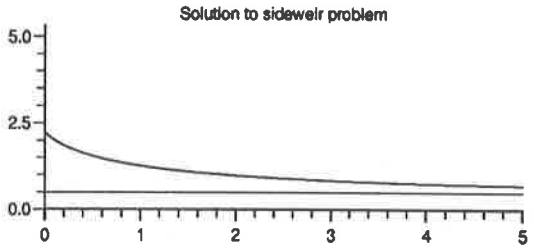

Figure 7: Depth for Problem 2. Inflow depth and massflow are 2.23097m and $14.7079 m^3 s^{-1}$.

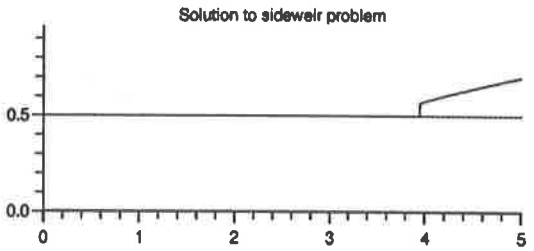

Figure 8: Depth for Problem 3. Inflow depth and massflow are 0.49985m and $1.22127 m^3 s^{-1}$. Froude no. is 1.2186.

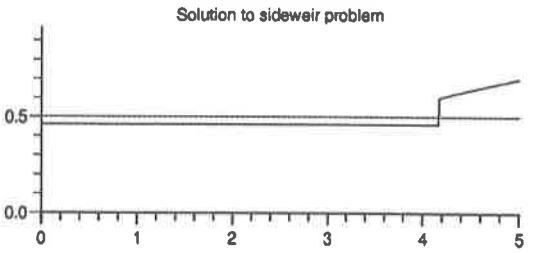

Figure 9: Depth for Problem 3a. Inflow depth and massflow are 0.4601987m and $1.1991996 m^3 s^{-1}$. Froude no. is 1.505637.

given rather trivially. This is what has happened in Problem 3, figure 8, where the smallest incoming Froude number that produces a physical flow is not 1 but 1.218. To demonstrate the non-uniqueness we search for a flow that has an incoming Froude number of 1.5, figure 9. This has the same outflow conditions, and indeed the sub-critical part of the two solutions is identical, but the super-critical part depends upon the boundary condition specified at inflow.

The calculation of the entirely sub-critical or entirely super-critical solution from (3.13) is quite trivial. The trans-critical case requires that we insert a jump on the sub-critical solution. The strength of the jump is determined for given sub-critical values of the depth and energy, y_2 and e_2 by the equations

$$\frac{y_2}{y_1} = \frac{1}{2}\left(\sqrt{1+8F_{r_1}^2}-1\right) \tag{3.14}$$

$$e_1 - e_2 = \frac{(y_2-y_1)^3}{4y_1y_2}. \tag{3.15}$$

The Froude number on the super-critical side, F_{r_1}, can be written in terms of the energy and depth on the super-critical side, e_1 and y_1, and hence we have two equations in two unknowns. It is perhaps easiest to solve (3.15) explicitly for e_1 and substitute this value into equation (3.14). This is not immediately solvable for y_1 but a simple bisection algorithm will converge to the solution rapidly and is very robust. Having obtained values of depth and energy corresponding to super-critical flow, the solution procedure can then proceed using (3.13) but with the new values. In practice, then, a sub-critical flow is calculated from outflow until we either reach inflow, in which case it is a purely

sub-critical flow, or until it becomes critical. At this point we construct a super-critical flow, using (3.14) and (3.15), and attempt to reach inflow. If the flow is not strong enough to reach inflow we take the next point back up the sub-critical solution and find the corresponding super-critical flow. We continue doing this until we either reach inflow (because of the monotonicity results of Porter [6] we know this will be the smallest jump capable of doing this) or we work our way right back to outflow being unable to find any physical jump resulting in a super-critical flow able to reach inflow. This is then one of the unphysical flow situations discussed at the end of the previous section. This procedure can be mirrored exactly in the numerical calculations.

3.1 Results for the One-Equation Model

The numerical solution to (3.12) proceeds along exactly similar lines to that for equation (1.4). Here the term $3y - 2e$ plays the role of $1 - F_r^2$ in (1.4). The terms that appear in the right-hand side are treated by the trapezium rule as in the iteration defined by (2.7). In figures 10—18 we see the results to Problem 1 with 1,2,4,8,16,32,64,128 and 256 points. A large number, 256, of iterations was performed in each test to try to eliminate this source of error.

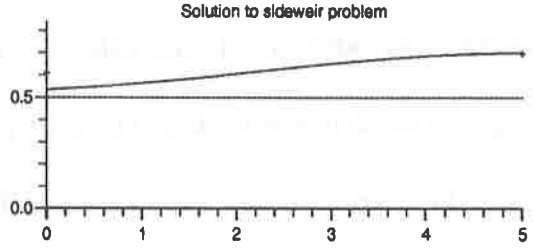

Figure 10: Depth for Problem 1 with 1 pt. Inflow depth and massflow are 0.61056m and $0.8091 m^3 s^{-1}$.

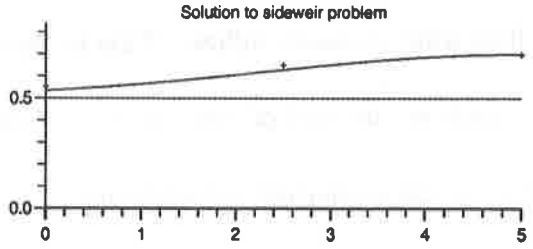

Figure 11: Depth for Problem 1 with 2 pts. Inflow depth and massflow are 0.55471m and $0.93611 m^3 s^{-1}$.

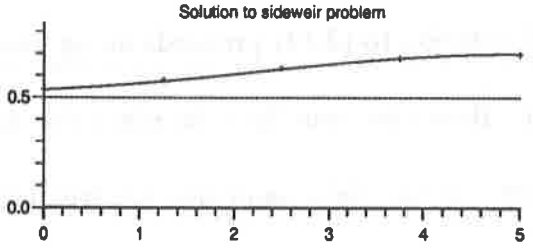

Figure 12: Depth for Problem 1 with 4 pts. Inflow depth and massflow are 0.53806m and $0.95863 m^3 s^{-1}$.

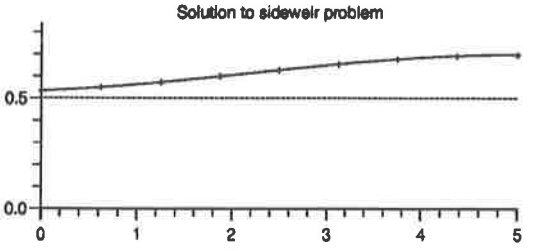

Figure 13: Depth for Problem 1 with 8 pts. Inflow depth and massflow are 0.535262m and $0.961845 m^3 s^{-1}$.

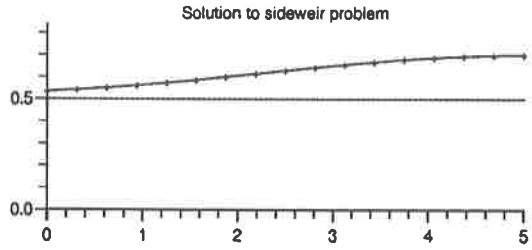

Figure 14: Depth for Problem 1 with 16 pts. Inflow depth and massflow are 0.534631m and $0.962548 m^3 s^{-1}$.

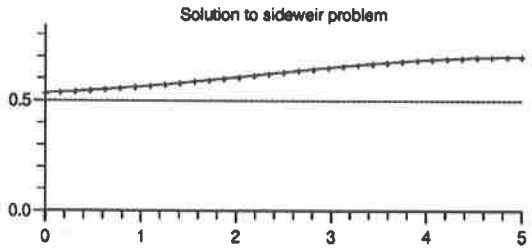

Figure 15: Depth for Problem 1 with 32 pts. Inflow depth and massflow are 0.534477m and $0.9627194 m^3 s^{-1}$.

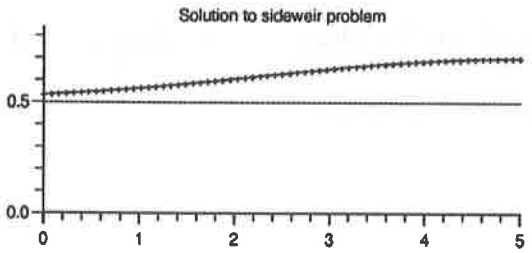

Figure 16: Depth for Problem 1 with 64 pts. Inflow depth and massflow are 0.534438m and $0.962762 m^3 s^{-1}$.

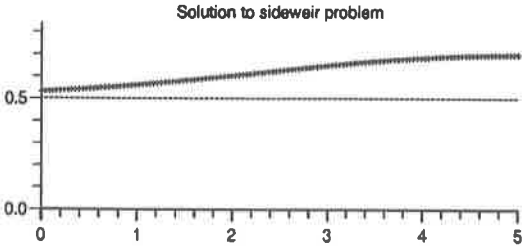

Figure 17: Depth for Problem 1 with 128 pts. Inflow depth and massflow are 0.534429m and $0.9627725 m^3 s^{-1}$.

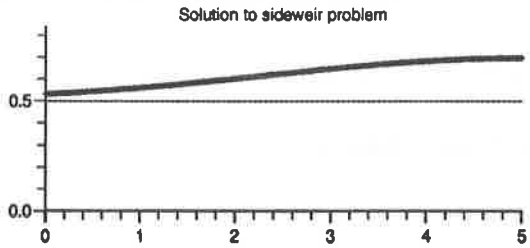

Figure 18: Depth for Problem 1 with 256 pts. Inflow depth and massflow are 0.534427m and $0.962775 m^3 s^{-1}$.

With just 8 points, figure 13, the solution appears, visually, to have converged. In table i we give the errors in the depth and massflow at inflow, the absolute value of the difference of the exact value and the value calculated by the scheme, and a calculation to determine the order of convergence based upon the results for depth.

No. of points	Error in depth	Error in massflow	Order of convergence
1	0.076134	0.153676	—
2	0.020284	0.026666	1.91
4	3.634×10^{-3}	4.146×10^{-3}	2.48
8	8.358×10^{-4}	9.308×10^{-4}	2.12
16	2.053×10^{-4}	2.28×10^{-4}	2.03
32	5.1×10^{-5}	5.66×10^{-5}	2.01
64	1.2×10^{-5}	1.41×10^{-5}	2.09
128	3×10^{-6}	3.5×10^{-6}	2.0
256	1×10^{-6}	1×10^{-6}	1.58

Table i: Errors for Problem 1 using the one equation model.

A similar set of results are now given for Problem 2. These are shown in figures 19—26. There is no solution with just one point. Visually the scheme has converged with 32 points.

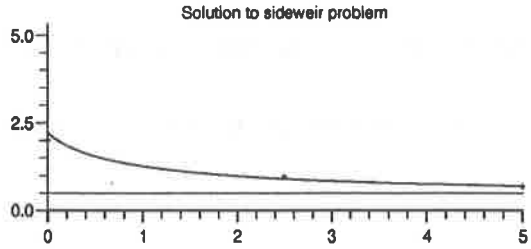

Figure 19: Depth for Problem 2 with 2 pts. Inflow depth and massflow are 2.014765m and $13.915011 m^3 s^{-1}$.

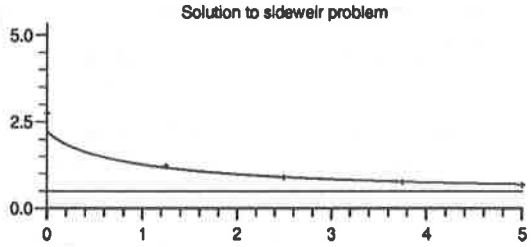

Figure 20: Depth for Problem 2 with 4 pts. Inflow depth and massflow are 2.767235m and $15.88488 m^3 s^{-1}$.

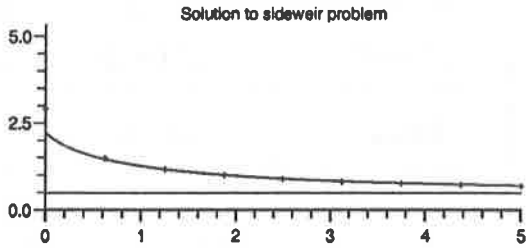

Figure 21: Depth for Problem 2 with 8 pts. Inflow depth and massflow are 2.9288m and $15.98409 m^3 s^{-1}$.

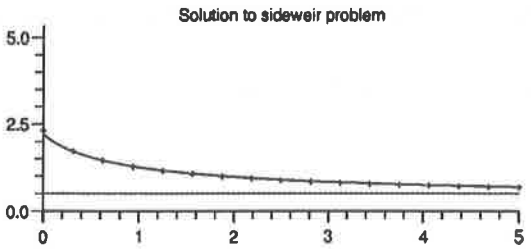

Figure 22: Depth for Problem 2 with 16 pts. Inflow depth and massflow are 2.327025m and $15.005198 m^3 s^{-1}$.

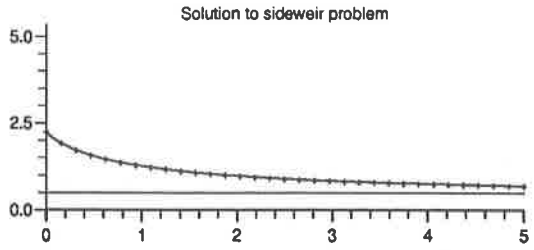

Figure 23: Depth for Problem 2 with 32 pts. Inflow depth and massflow are 2.25188m and $14.77559 m^3 s^{-1}$.

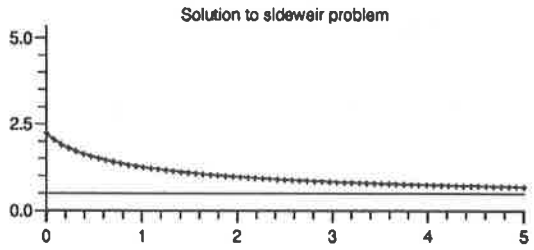

Figure 24: Depth for Problem 2 with 64 pts. Inflow depth and massflow are 2.23605m and $14.724497 m^3 s^{-1}$.

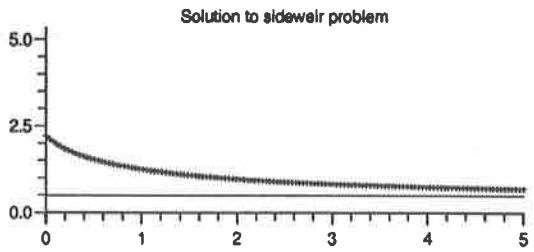

Figure 25: Depth for Problem 2 with 128 pts. Inflow depth and massflow are 2.232234m and $14.71203 m^3 s^{-1}$.

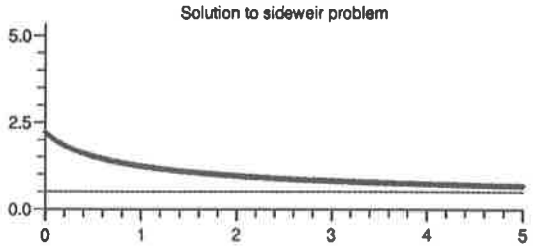

Figure 26: Depth for Problem 2 with 256 pts. Inflow depth and massflow are 2.231287m and $14.708932 m^3 s^{-1}$.

The results are summarised in table ii. Note that convergence does not take place until a certain level of refinement takes place.

No. of points	Error in depth	Error in massflow	Order of convergence
1	Iteration	diverged	—
2	0.216205	0.792889	—
4	0.536265	1.17698	—
8	0.69783	1.27619	—
16	0.096055	0.297298	2.86
32	0.02091	0.06769	2.19
64	5.08×10^{-3}	0.016597	2.04
128	1.264×10^{-3}	4.13×10^{-3}	2.0
256	3.17×10^{-4}	1.032×10^{-3}	2.0

Table ii: Errors for Problem 2 using the one equation model.

Finally we look at the trans-critical problem, Problem 3. The results for this are shown in figures 27—35. Here 64 points, figure 33, are needed for visual convergence. A compendium of the results is also given in table iii.

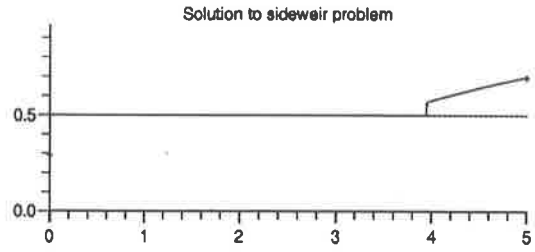

Figure 27: Depth for Problem 3 with 1 pt. Inflow depth and massflow are 0.2934634m and $1.0m^3s^{-1}$.

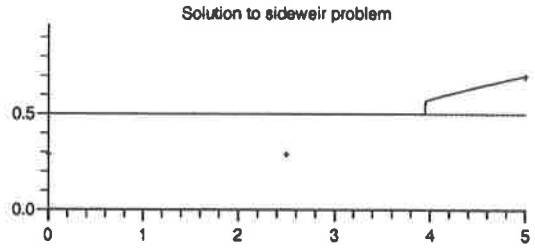

Figure 28: Depth for Problem 3 with 2 pts. Inflow depth and massflow are 0.2934634m and $1.0m^3s^{-1}$.

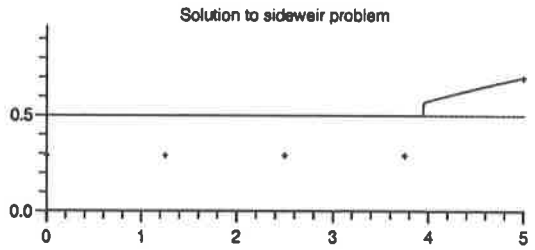

Figure 29: Depth for Problem 3 with 4 pts. Inflow depth and massflow are 0.2934634m and $1.0m^3s^{-1}$.

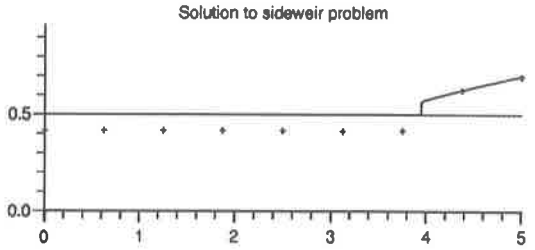

Figure 30: Depth for Problem 3 with 8 pts. Inflow depth and massflow are 0.4191594m and $1.164498m^3s^{-1}$.

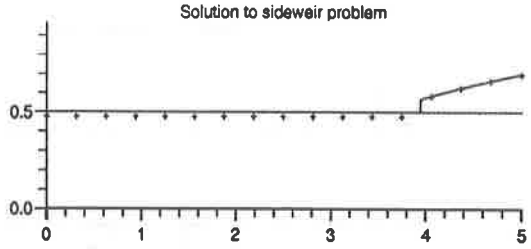

Figure 31: Depth for Problem 3 with 16 pts. Inflow depth and massflow are 0.478354m and $1.210861 m^3 s^{-1}$.

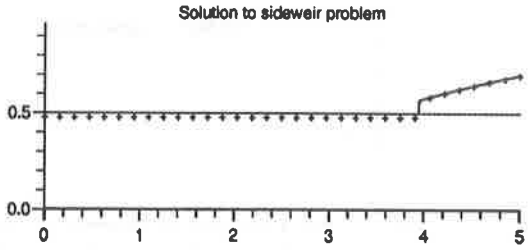

Figure 32: Depth for Problem 3 with 32 pts. Inflow depth and massflow are 0.47917657m and $1.2113295 m^3 s^{-1}$.

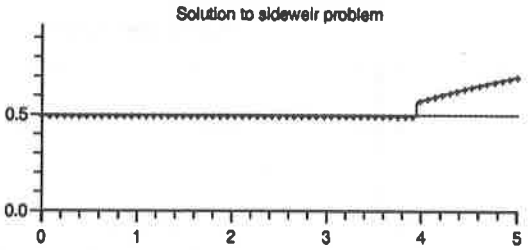

Figure 33: Depth for Problem 3 with 64 pts. Inflow depth and massflow are 0.493434m and $1.2185766 m^3 s^{-1}$.

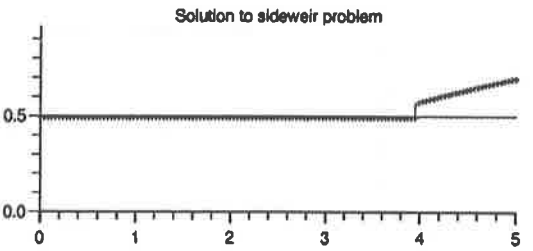

Figure 34: Depth for Problem 3 with 128 pts. Inflow depth and massflow are 0.4934964m and $1.218604 m^3 s^{-1}$.

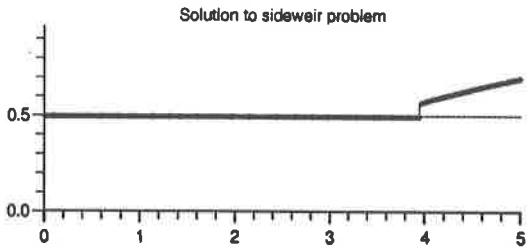

Figure 35: Depth for Problem 3 with 256 pts. Inflow depth and massflow are 0.4971m and $1.2201566 m^3 s^{-1}$.

No. of points	Error in depth	Error in massflow	Order of convergence
1	0.2063866	0.22127	—
2	0.2063866	0.22127	—
4	0.2063866	0.22127	—
8	0.0806906	0.056772	1.35
16	0.021496	0.010409	1.91
32	0.02067343	9.9405×10^{-3}	0.06
64	6.416×10^{-3}	2.6934×10^{-3}	1.69
128	6.3536×10^{-3}	2.666×10^{-3}	0.01
256	2.75×10^{-3}	1.1134×10^{-3}	1.21

Table iii: Errors for Problem 3 using the one equation model.

The scheme shows a definite 2^{nd} order convergence in the case of entirely sub-critical or entirely super-critical flow, tables i and ii. In the trans-critical case, table iii, the convergence is now only first order. This is to be expected because the approximation to the jump position is only first order and this dominates the error in Problem 3.

We now look at the convergence rate of the iteration. For this we consider Problem 2 with 64 points. The solutions with different numbers of iterations are shown in figures 36—43.

Table iv shows the errors and convergence of the sequence of solutions.

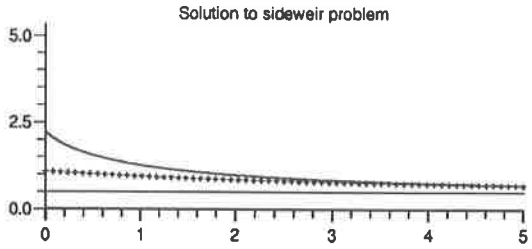

Figure 36: Depth for Problem 2 with 1 iteration. Inflow depth and massflow are 1.102355m and $8.927252 m^3 s^{-1}$.

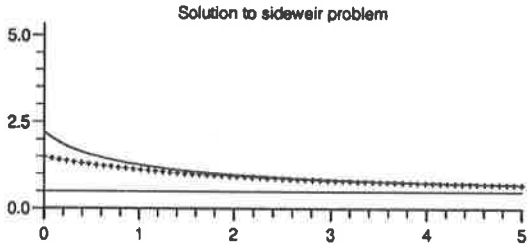

Figure 37: Depth for Problem 2 with 2 iterations. Inflow depth and massflow are 1.498345m and $11.3935138 m^3 s^{-1}$.

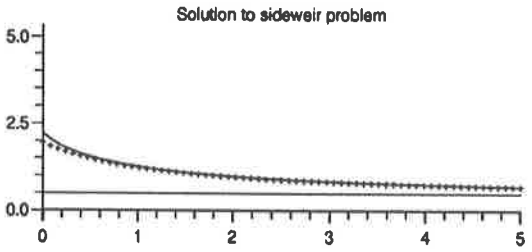

Figure 38: Depth for Problem 2 with 4 iterations. Inflow depth and massflow are 1.9567117m and $13.6743 m^3 s^{-1}$.

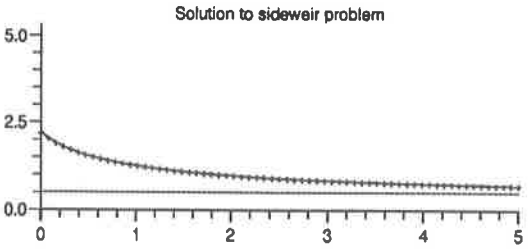

Figure 39: Depth for Problem 2 with 8 iterations. Inflow depth and massflow are 2.185106m and $14.55374 m^3 s^{-1}$.

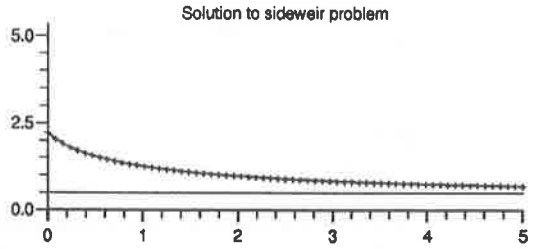

Figure 40: Depth for Problem 2 with 16 iterations. Inflow depth and massflow are 2.232427m and $14.712664 m^3 s^{-1}$.

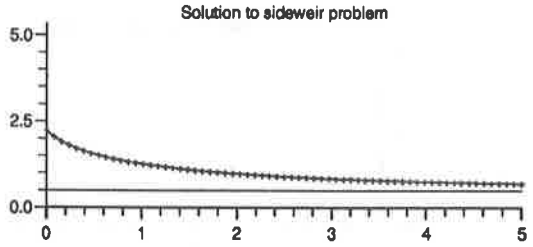

Figure 41: Depth for Problem 2 with 32 iterations. Inflow depth and massflow are 2.236011m and $14.724362 m^3 s^{-1}$.

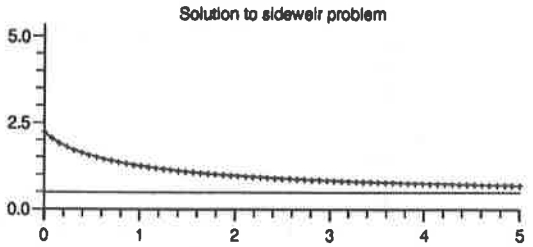

Figure 42: Depth for Problem 2 with 64 iterations. Inflow depth and massflow are 2.236053m and $14.724497 m^3 s^{-1}$.

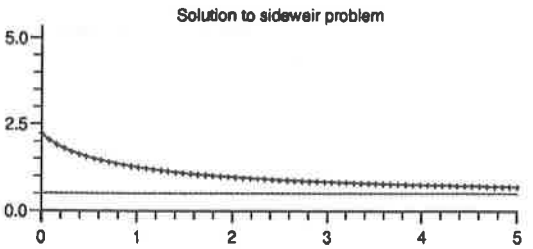

Figure 43: Depth for Problem 2 with 128 iterations. Inflow depth and massflow are 2.236053m and $14.724497 m^3 s^{-1}$.

No. of iterations	Error in depth	Error in massflow	Order of convergence
1	1.133698	5.797245	—
2	0.737708	3.3309832	0.62
4	0.2793413	1.050197	1.40
8	0.050947	0.170757	2.45
16	3.626×10^{-3}	0.011833	3.81
32	4.2×10^{-5}	1.35×10^{-4}	6.43
64	0.0	0.0	—
128	0.0	0.0	—

Table iv: Errors for Problem 2 using the one equation model.

From these results it is very difficult to give any firm conclusions as to the order of the iteration. It does, however, seem to start as a low order convergence and then rapidly accelerates as the exact answer is approached.

Clearly it is best to use as many space steps and as many iterations as one can, but as a rough guide it would seem that between 40 and 50 space steps are needed per metre to give robust results. This gives excessive accuracy for the sub-critical case, more than adequate accuracy for the super-critical case and 'robust' accuracy for the trans-critical case. Around 10 iterations seems also to lead to robust accuracy. These observations also hold for the two-equation model. Since the emphasis is on having a robust code it is better to refine in the spacial step, rather than the number of iterations, because this then guarantees better accuracy in the trans-critical case.

3.2 Results for the Two-Equation Model

We have now seen that the IDES technique can solve side-weir problems governed by (3.12) for all flow regimes. For the purposes of CHAT, though, we cannot assume zero slope together with the other assumptions, in particular zero friction, used to derive (3.12). This means that we will need to solve equations (3.9) and (3.10) as a system . Equation (3.9) is discretised in an identical manner to that described for (3.12) and (2.6) before. At the same time we discretise (3.10) using the trapezium rule with the implicit terms on the right-hand side again lagged, that is, using the previous iteration value, to give an explicit expression for the new value Q^{k+1}. We have updated (3.10) first and then used the latest value of Q^{k+1} to update y^{k+1} from the discretisation of (3.9). This choice seems to have no effect on the scheme. To validate this approach Problem 2 is again solved but this time with the two-equation model, that is without assuming constant energy. These results are shown in figures 44—49. Errors, as before, are shown in table v.

The order of the scheme is again definitely shown to be 2. Comparing with the results in table ii we see that the errors are very comparable, being slightly better for the depth and slightly worse for the massflow. Although it does not show up clearly in figures 44 to 49, the energy is no longer constant, as we would expect since this is no longer enforced. Also we are not able to calculate a solution on some of the coarser meshes.

No. of points	Error in depth	Error in massflow	Order of convergence
8	0.3470903	1.694867	—
16	0.0610075	0.3181655	2.51
32	0.014248	0.076558	2.10
64	3.5011×10^{-3}	0.01904	2.02
128	8.72×10^{-4}	4.757×10^{-3}	2.01
256	2.18×10^{-4}	1.19×10^{-3}	2.00

Table v: Errors for Problem 2 using the two equation model.

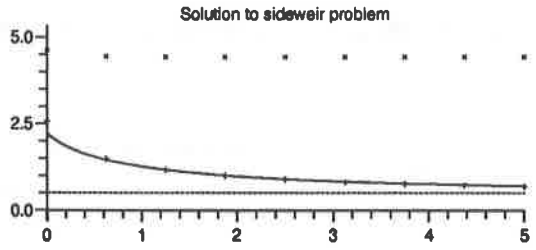

Figure 44: Depth and energy for Problem 2 with 8 pts. Inflow depth and massflow are 2.5780623m and $16.402767m^3s^{-1}$. Two equation model.

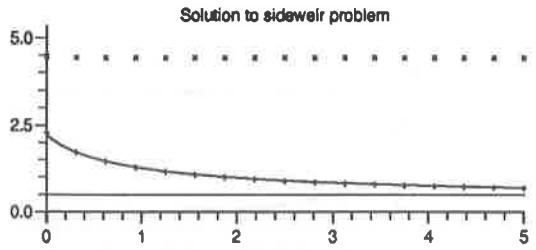

Figure 45: Depth and energy for Problem 2 with 16 pts. Inflow depth and massflow are 2.2919795m and $15.0260655m^3s^{-1}$. Two equation model.

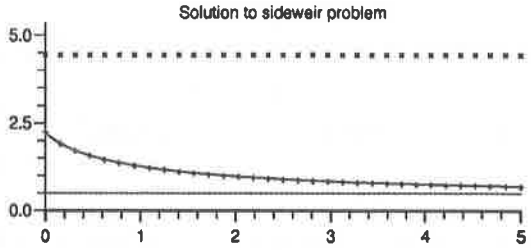

Figure 46: Depth and energy for Problem 2 with 32 pts. Inflow depth and massflow are 2.24522m and $14.784458 m^3 s^{-1}$. Two equation model.

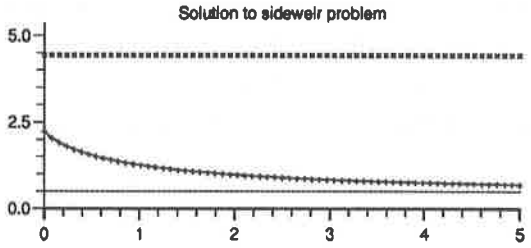

Figure 47: Depth and energy for Problem 2 with 64 pts. Inflow depth and massflow are 2.2344731m and $14.72694 m^3 s^{-1}$. Two equation model.

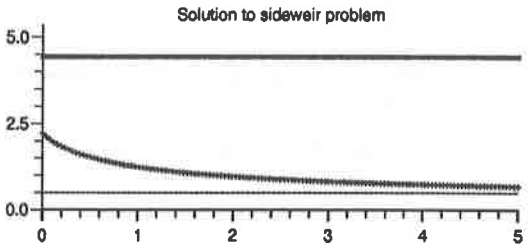

Figure 48: Depth and energy for Problem 2 with 128 pts. Inflow depth and massflow are 2.231844m and $14.712657 m^3 s^{-1}$. Two equation model.

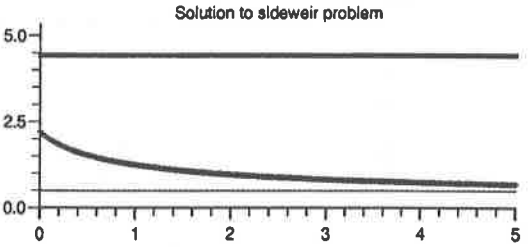

Figure 49: Depth and energy for Problem 2 with 256 pts. Inflow depth and massflow are 2.23119m and $14.70909 m^3 s^{-1}$. Two equation model.

The main advantage of the two-equation model is that we are not constrained by the assumptions needed to create (3.12). We now look at some more complicated examples to demonstrate this. All these examples have the same parameters as for Problem 1 except that there is now a bed-slope of 0.02. In Problem 4, figure 50, there is a constant breadth of 0.75m. The inflow depth and massflow are $0.447m$ and $0.58083m^3s^{-1}$. For Problem 5, figure 51, the breadth now varies from 0.5m at inflow to 1m at outflow. The inflow depth and massflow for this case are $0.43736m$ and $0.533m^3s^{-1}$. Finally in Problem 6, figure 52, the breadth varies from 1m at inflow to 0.5m at outflow.

Results have also been obtained for non-zero friction, $\alpha \neq 1$, and for channels with more than one side-weir. (This just involves multiplying the right-hand side of (3.10) by the number of side-weirs.) All the results were as to be expected.

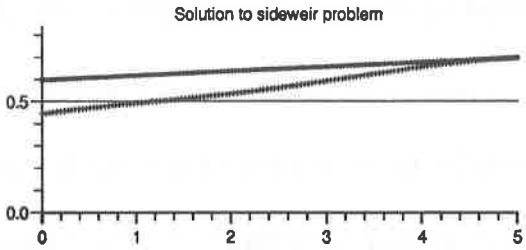

Figure 50: Depth and energy for Problem 4 with 128 pts. and 10 iterations.

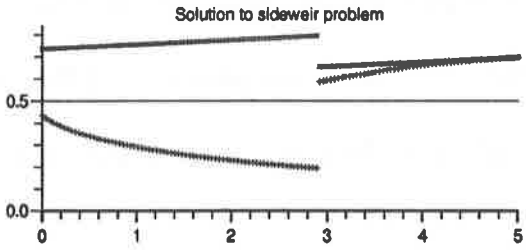

Figure 51: Depth and energy for Problem 5 with 128 pts. and 10 iterations.

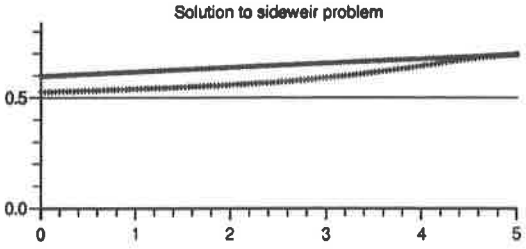

Figure 52: Depth and energy for Problem 6 with 128 pts. and 10 iterations.

4 Conclusions

We have shown the IDES method to be quite capable of solving the type of channel flows and side-weir flows to be encountered in CHAT. Sub-critical and super-critical flows can be solved to second-order accuracy and a procedure for obtaining one of the physical solutions in the trans-critical case has been explained and shown to be effective. Possible procedures for dealing with the two types of unphysical flow to be encountered have also been discussed. Bed-slopes, varying widths, etc. can all be included in the scheme and it has been shown to work with these extra terms also included.

Equation (3.10) is the discharge law for a side-weir. However, the methodology is not reliant upon this form of law and others may be used. For example, the case of a channel with a rack in the bed could be solved using the same code with a changed discharge law.

Perhaps one flaw with this work is the number of space-steps needed to guarantee robust results. Although entirely sub-critical and entirely super-critical flows can be resolved with rather few points the number has to be kept sufficiently large in order that the trans-critical case is resolved accurately. The scheme is still fairly quick but there is hope for future improvements in its efficiency by using grid adaption. One pointer to the fact that this may be possible is the fact that in Problem 3 results of the right kind were obtained on very coarse meshes, figures 27—30; they were just rather inaccurate. Whether the logic required to implement an adaptive scheme will be that much quicker than

just using a finer fixed mesh is an open question. It is also worth noting that the discontinuous nature of the solution was picked up on the coarse grids and it must be remembered that these solutions are just as valid physically as the one we were aiming for, which was the one with the smallest jump. If there is no strong reason for choosing this particular solution then the coarse grid results are just as physically valid and the number of points per metre can be reduced to, say, between 10 and 15.

5 Acknowledgments

The author wishes to acknowledge the cooperation of Drs. Roland Price and John Wixcey of HR Wallingford in suggesting the problems solved in this report and for their general help and also to Drs. Dave Porter and Mike Baines for many interesting discussions about aspects of this work. The work was sponsored by HR Wallingford, whom the author would also like to thank.

References

[1] Chawdhary, K.S., *"On the Solution of Implicit First-Order Differential Equations."* M.Sc. Dissertation, Dept. of Mathematics, University of Reading, 1991.

[2] Chow, V.T., *"Open-Channel Hydraulics."* McGraw Hill, 1959.

[3] Fox, L. & Mayers, D.F., *"On the Numerical Solution of Implicit Ordinary Differential Equations."* IMA J. Numer. Anal., **1**, pp. 377-401, 1981.

[4] Henrici, P., *"Discrete Variable Methods in Ordinary Differential Equations."* John Wiley & Sons, 1962.

[5] Lambert, J.D., *"Computational Methods in Ordinary Differential Equations."* John Wiley & Sons, 1973.

[6] Porter, D., *Private Communication,* Dept. of Mathematics, University of Reading, 1992.

[7] Samuels, P.G. & Chawdhary, K.S., *"A Backwater Method for Trans-Critical Flows."* 2^{nd} Int. Conf. on Hydraulic & Environmental Modelling of Coastal,

Estuarine and River Waters, University of Bradford, 22-24 September 1992.